

Kinetics of methane oxidation over La–Sr–Ce–Fe–O mixed oxide solids

V. C. Belessi, A. K. Ladavos, G. S. Armatas and P. J. Pomonis*

Department of Chemistry, University of Ioannina, Ioannina 45110, Greece.
E-mail: ppomonis@cc.uoi.gr

Received 17th April 2001, Accepted 24th June 2001

First published as an Advance Article on the web 30th July 2001

A kinetic study of methane combustion over $\text{La}_{0.7}\text{Ce}_{0.3}\text{FeO}_3$, $\text{La}_{0.7}\text{Sr}_{0.3}\text{FeO}_3$ and $\text{La}_{0.7}\text{Sr}_{0.1}\text{Ce}_{0.2}\text{FeO}_3$ mixed oxide solids has been carried out. From kinetic analyses of reaction rate, the combustion can be expressed by the Rideal–Eley mechanism, in which adsorbed oxygen, in dissociative form, is assumed to react with gaseous methane. True activation energies E_{true} , in the range 63–75 kJ mol^{-1} , and heats of adsorption of oxygen λ_{O_2} , in the range 53–211 kJ mol^{-1} , have been determined. The large values of λ_{O_2} , are related to existence of a $\text{SrFeO}_{3\pm x}$ perovskite crystal phase, which is able to uptake large amounts of oxygen.

Introduction

The catalytic combustion of hydrocarbons at low temperatures is one of the ways to reduce the formation of nitrogen oxides compared with conventional combustion in air atmosphere which takes place at temperatures up to 1300 °C. Towards this end, several catalytic materials have been tested in a number of laboratories worldwide.¹ The combustion at low temperatures is assured by highly active catalysts, such as supported noble metals, which so far are used almost exclusively, although more economical and possibly more poison-resistant substitutes, particularly from the group of transition metal oxides, have been actively sought for more than three decades. Among them perovskite oxides appear to be some of the most promising candidates, owing to the fact that they guarantee a fair catalytic activity and stability at comparatively high temperatures.^{2–5} The early lanthanide perovskites, particularly LaBO_3 (B = first-row transition metal) have received the most attention for catalytic combustion of hydrocarbons. In the majority of studies the identity of the B cation has a large influence on the catalytic activity. Single $\text{La}_{1-x}\text{A}_x\text{BO}_{3\pm\delta}$ or doubly $\text{La}_{1-x}\text{A}_x\text{B}_{1-y}\text{B}_y\text{O}_{3\pm\delta}$ substituted perovskites have been also extensively tested^{6–10} and synergistic effects, showing superior performance in the case of mixed materials, have been reported in most cases.^{11,12} In the vast majority of these studies, catalytic rates were examined at a single gas composition or only in terms of light-off temperatures. On the contrary, full kinetic studies of methane combustion were obtained only in a small number of cases.^{6,7,10,13}

There is no single consistent mechanism that describes adequately the kinetics of oxidation of alkanes, alkenes, aromatics, oxygenates *etc.* over typical VOC oxidation catalysts such as noble metals or perovskites. The investigation of complete oxidation of C_1 – C_4 alkanes over Pt, Pd and Rh catalysts carried out by Yao¹⁴ showed various reaction mechanisms and the reaction orders for hydrocarbon and oxygen varies for different molecules and catalysts. Kinetic analyses of reaction rate data over Pt/alumina are consistent with a Langmuir–Hinshelwood mechanism, in which the chemisorbed oxygen reacts with adsorbed methane molecules.^{6,15} In many investigations it has been proposed that the oxidation over per-

ovskite oxides proceeds by both suprafacial and intrafacial reactions.² In the suprafacial process the reaction rate appears to be correlated primarily with the electronic configurations of the surface transition-metal ions or the surface defects. In this case the reaction takes place between the adsorbed species on the surface at relatively low temperatures. Conversely, the intrafacial mechanism takes over at high temperatures and the reaction rate appears to be correlated primarily with the thermodynamic stability of oxygen vacancies adjacent to a transition-metal ion.^{2,4,6,13} However, the role of these oxygen species in complete and selective oxidation and their participation in combustion over various ceramic perovskite phases is still an open question. On the other hand, the Mars and Van Krevelen (MVK) redox model assumes that the supply of oxygen from the gas phase is irreversible, and occurs only when a reduced site is made available by the reaction, allowing site oxidation to be a limiting factor in the kinetics.^{7,10}

Arai *et al.*⁶ compared the catalytic oxidation of methane over various La–Mn perovskite-type oxides with Pt/alumina catalyst. From kinetic analyses of the reaction rate, the oxidation on Pt/alumina can be expressed by the Langmuir–Hinshelwood mechanism, in which the adsorbed oxygen plays a major role. On the other hand, weakly bonded adsorbed oxygen dominantly participates in the reaction on perovskite oxides at low temperatures, and this oxygen desorbs with increasing temperature. The lattice oxygen becomes reactive at high temperatures after thermal desorption of adsorbed oxygen.

The reaction rate of methane combustion over $\text{La}_{2-x}\text{Sr}_x\text{NiO}_{4-\lambda}$ ¹³ solids was found to consist of two rate components, one suprafacial, employing oxygen from the gas phase and active at low temperatures, and another intrafacial, employing oxygen from the perovskite lattice and apparent mainly at high temperatures. The reaction dependence was first order relative to methane while the reaction order for oxygen decreases from 0.5 to 0.2 as the temperature increases.

Klvana *et al.*¹⁰ examined two kinetic models, for the kinetic study of methane combustion over $\text{La}_{0.66}\text{Sr}_{0.34}\text{Ni}_{0.3}\text{Co}_{0.7}\text{O}_3$ and $\text{La}_{0.4}\text{Sr}_{0.6}\text{Fe}_{0.4}\text{Co}_{0.6}\text{O}_3$ perovskites. A simple first order model $r = kP_{\text{CH}_4}$ and a two-term model $r = (k_1 + k_2P_{\text{O}_2}^{0.5})P_{\text{CH}_4}$, were tested. The first order model gave a good fit to the experimental data for $\text{La}_{0.66}\text{Sr}_{0.34}\text{Ni}_{0.3}\text{Co}_{0.7}\text{O}_3$ and

was also found to be adequate for $\text{La}_{0.4}\text{Sr}_{0.6}\text{Fe}_{0.4}\text{Co}_{0.6}\text{O}_3$. However, in the case of the latter catalyst the experimental data was best described by a MVK model.

Stojanovic *et al.*⁷ found that the catalytic activity for methane oxidation over $\text{LaCr}_{1-x}\text{Ni}_x\text{O}_4$ increases monotonically with the value of x . The kinetics behaviour correlated well with an oxidation–reduction mechanism, similar to that proposed by the MVK model, for all catalysts, proposing Ni–O–Ni ensembles as the key surface reagents.

$\text{LaMn}_{1-x}\text{Mg}_x\text{O}_3$ perovskite catalysts were tested for the deep oxidation of methane by Saracco *et al.*¹⁶ A Rideal–Eley mechanism fitted satisfactorily the experimental kinetics for LaMnO_3 and Mg-doped LaMnO_3 . However, as opposed to LaMnO_3 , the catalytic combustion over $\text{LaMn}_{0.8}\text{Mg}_{0.2}\text{O}_3$ seemed to involve two different types of adsorbed oxygen species, depending on the operating temperature.

Although the above studies give a good account of kinetics for deep oxidation of methane over noble metals and ceramic catalysts, various questions remain. Namely, in some of the cases mentioned above^{6,7,10,13,16} apparent activation energies were calculated while in fewer cases true activation energies were also found.^{6,10,13,14} Is there perhaps any internal consistency between those results? Another interesting question is what is the meaning of apparent reaction orders found for methane and oxygen^{6,7,13} and how are they related to the more formal Langmuir–Hinshelwood or Rideal–Eley kinetic models? Are perhaps those apparent reaction orders, representing kinetic parameters, somehow related to the strength of adsorption of the reacting species, *i.e.* to thermodynamic parameters? And if so what can this relationship be?

The aim of this paper is a detailed kinetic study of the methane combustion over the mixed oxide perovskites $\text{La}_{0.7}\text{Ce}_{0.3}\text{FeO}_3$, $\text{La}_{0.7}\text{Sr}_{0.3}\text{FeO}_3$ and $\text{La}_{0.7}\text{Sr}_{0.1}\text{Ce}_{0.2}\text{FeO}_3$. Such solids are members of a more extensive series with general formulae $\text{La}_{1-x-y}\text{Sr}_x\text{Ce}_y\text{FeO}_3$ studied recently by the present group; the relevant results have been published previously elsewhere.^{17,18}

Experimental

Methods of catalysts preparation and characterization

The tested catalysts $\text{La}_{0.7}\text{Sr}_{0.3}\text{FeO}_3$, $\text{La}_{0.7}\text{Ce}_{0.3}\text{FeO}_3$ and $\text{La}_{0.7}\text{Sr}_{0.1}\text{Ce}_{0.2}\text{FeO}_3$ can be considered as members of the three sub-groups of the series $\text{La}_{1-x-y}\text{Sr}_x\text{Ce}_y\text{FeO}_3$ with the nominal formulae $\text{La}_{1-x}\text{Sr}_x\text{FeO}_3$, $\text{La}_{1-y}\text{Ce}_y\text{FeO}_3$ and $\text{La}_{1-x-y}\text{Sr}_x\text{Ce}_y\text{FeO}_3$. Details about the preparation method

for the whole series are given in ref. 17. Briefly, calculated amounts of $\text{La}(\text{NO}_3)_3 \cdot 6\text{H}_2\text{O}$ (Merck), $\text{Fe}(\text{NO}_3)_3 \cdot 9\text{H}_2\text{O}$ (Merck), $\text{Sr}(\text{NO}_3)_2$ (Ferak) and CeO_2 (Aldrich) were mixed thoroughly in an agate mortar and heated slowly up to 400 °C for complete nitrate decomposition. The mixtures were further heated at 900 °C for 4 h under atmospheric conditions. Then the mixtures were cooled and ground in an agate mortar and heated again at 1050 °C for a further 4 h. The solids obtained after grinding were checked for their structural properties.

The specific surface area of the solids, after the final heating, was checked by N_2 adsorption at 77 K in a conventional Fisons 1900 Sorptomatic apparatus. The values found were low, 1–4 $\text{m}^2 \text{g}^{-1}$, as expected.

The crystal structure of the prepared materials was determined by XRD analysis using a SIEMENS Diffract 500 system employing $\text{CuK}\alpha$ radiation ($\lambda = 1.5418 \text{ \AA}$). Details of the corresponding XRD patterns are included in refs. 17 and 18. ^{57}Fe Mössbauer spectra were obtained for the three samples at 300 and 20 K, using a closed loop refrigerator system. The spectrometer was calibrated with $\alpha\text{-Fe}$ and isomer shift values are given relative to this. The experimental data were fitted by a least-squared computer minimization routine using a sum of spectral components characterizing different iron phases.¹⁹

Table 1 shows the catalysts used together with some of their structural characteristics as determined and published previously.^{12,17,18}

CH_4 combustion kinetics

The kinetics experiments were carried out in a bench scale tubular plug flow reactor (PFR), at 1 atm total pressure, connected to a gas chromatograph (GC) for analyses. Catalysts were activated at 500 °C for 1 h in 60 ml min^{-1} helium flow. After cooling to 400 °C, a mixture of $\text{CH}_4/\text{O}_2/\text{He}$, at a total flow rate of 115 ml min^{-1} , was passed through the catalyst bed containing 0.25 g of the catalyst. Variation of the partial pressures of oxygen and methane, using suitable controls and flow meters, was possible to calculate the dependence of the reaction rate on the partial pressures P_{CH_4} and P_{O_2} . The used partial pressure values are listed in Table 2. The catalysts were active from $\theta = 440 \text{ }^\circ\text{C}$ and the conversions of CH_4 were checked at intervals of 20 °C up to 620 °C. Analyses of the reactants and products were carried out by sampling 1 ml of the gases to a Shimadzu 15 A GC equipped with a TCD, with He as carrier gas and connected to a Chromatopak C-R6A integrator system. The column used for analysis was a 60/80 Carboxen 1000 (15' \times 1/8", s.s. supplied by Supelco). The

Table 1 Catalysts used, crystal phases as found by XRD and percentage of iron-containing crystal phases as found by Mössbauer spectroscopy at 20 K

Catalyst	Crystal phases as found by XRD	Crystal phases (%) as found by Mössbauer spectroscopy at 20 K
$\text{La}_{0.7}\text{Ce}_{0.3}\text{FeO}_3$	$\text{LaFeO}_3/\text{Fe}_2\text{O}_3/\text{CeO}_2/\text{La}(\text{OH})_3^a$	LaFeO_3 64 Fe_2O_3 36
$\text{La}_{0.7}\text{Sr}_{0.3}\text{FeO}_3$	$\text{LaFeO}_3/\text{SrFeO}_{3-x}/\text{SrFeLaO}_4^a/\text{La}(\text{OH})_3^a/\text{SrFe}_{12}\text{O}_{19}^a$	LaFeO_3 39 Fe_2O_3 28 $\text{SrFeO}_{3\pm x}$ 33
$\text{La}_{0.7}\text{Sr}_{0.1}\text{Ce}_{0.2}\text{FeO}_3$	$\text{LaFeO}_3/\text{SrFeO}_{3-x}/\text{Fe}_2\text{O}_3/\text{CeO}_2/\text{La}(\text{OH})_3^a/\text{SrFe}_{12}\text{O}_{19}^a$	LaFeO_3 55 Fe_2O_3 33 $\text{SrFeO}_{3\pm x}$ 12

^a Trace amounts.

Table 2 Partial pressures of methane (P_{CH_4}) and of oxygen (P_{O_2}) used for the determination of kinetics of methane oxidation

$P_{\text{CH}_4}/\text{atm}$	0.017	0.026	0.035	0.043	0.052	0.035	0.035	0.035	0.035	0.035
$P_{\text{O}_2}/\text{atm}$	0.07	0.07	0.07	0.07	0.07	0.035	0.052	0.070	0.087	0.104
$\theta/^\circ\text{C}$	For each pair of pressures (P_{CH_4} , P_{O_2}) the conversion was examined at $\theta = 440, 460, 480, 500, 540, 580$ and $620 \text{ }^\circ\text{C}$									

system was heated externally *via* a tubular furnace, regulated by a SUR BERLIN controller, within $\pm 1^\circ\text{C}$, *via* a thermocouple in contact with the catalyst bed. The carrier gas flow was kept at 30 ml min^{-1} and the only detected products were CO_2 and H_2O . In each experiment the integral reaction rates were calculated as the amount (μmol) reacted per unit time and unit mass.

Results

The obtained experimental data were treated using various models, such as adsorption of oxygen in dissociative or non-dissociative form, adsorption or no adsorption of methane on the surface, adsorption of oxygen and methane at distinct sites, and reaction rates made up of one suprafacial mechanism using oxygen from the gas phase plus a second intrafacial mechanism at higher temperatures using oxygen from the solid. We also treated the data phenomenologically as shown below. In all cases describing formal kinetics, treatment took place using a suitable computer program,²⁰ written in FORTRAN, based on the well-known 'Simplex' method.^{21,22} The criterion used to choose the best cases was the least sum of square errors (SSE) of the simulation curves with the experimental data. At the end we found that the best fitting was achieved using Rideal–Eley kinetics. Apart from this case, the mis-fitting example of the well-known Langmuir–Hinshelwood kinetics is shown, as well as the phenomenological kinetics. The purpose of this was to correlate, eventually, the phenomenological reaction orders of methane and oxygen with the thermodynamic parameters of adsorption, as will be discussed in the last part of the paper.

Phenomenological dependence of oxidation rate on the partial pressures of O_2 and CH_4

In a first approach the reaction kinetics of methane oxidation over the three catalysts, $\text{La}_{0.7}\text{Ce}_{0.3}\text{FeO}_3$, $\text{La}_{0.7}\text{Sr}_{0.3}\text{FeO}_3$ and $\text{La}_{0.7}\text{Sr}_{0.1}\text{Ce}_{0.2}\text{FeO}_3$, were examined by changing the partial pressures of oxygen and methane. The results were expressed by the empirical rate equation

$$R = k(P_{\text{CH}_4})^m(P_{\text{O}_2})^n \quad (1)$$

where R is the oxidation rate of methane and m and n are the apparent reaction orders for methane and oxygen, respectively. Phenomenological rate equations similar to eqn. (1) have been used in the past by various groups.^{6,7,13} Then, taking logarithms, eqn. (1) obtains the form

$$\ln R = \ln k' + m \ln P_{\text{CH}_4} + n \ln P_{\text{O}_2} \quad (2)$$

The graphical representation of $\ln R = f(\ln P_{\text{CH}_4})$ at T , $P_{\text{O}_2} = \text{constant}$ and/or $\ln R = f(\ln P_{\text{O}_2})$ at T , $P_{\text{CH}_4} = \text{constant}$, should give straight lines with slopes m and n respectively. Good straight lines with correlation coefficients approaching unity were obtained in all cases. Typical results are shown in Fig. 1.

The calculated values of m and n corresponding to the phenomenological reaction orders, are summarized in Table 3.

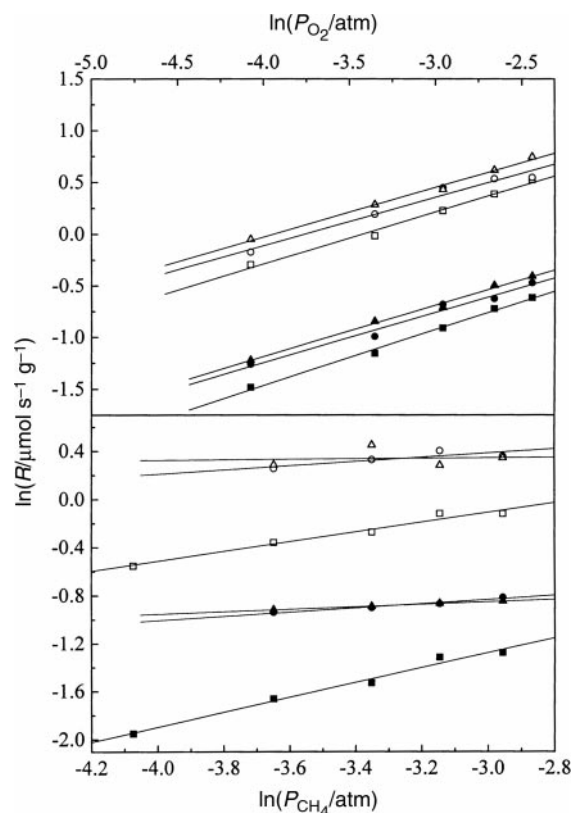


Fig. 1 Graphical representation of eqn. (2) for the calculation of phenomenological reaction orders n and m . Points: experimental; lines: best fittings using first order equations. Solid symbols: 440°C , open symbols: 500°C . Squares: $\text{La}_{0.7}\text{Ce}_{0.3}\text{FeO}_3$, circles: $\text{La}_{0.7}\text{Sr}_{0.3}\text{FeO}_3$ and triangles: $\text{La}_{0.7}\text{Sr}_{0.1}\text{Ce}_{0.2}\text{FeO}_3$.

The catalysts showed nearly first order kinetics with respect to methane with m around 0.7–0.8 in most cases. On the other hand, the exponents, n , for oxygen were much smaller and that for solid La–Sr–Fe–O was around 0.10–0.15 in most cases. For the La–Ce–Fe–O material the values were somewhat larger, in the range 0.3–0.4. Finally, for the La–Sr–Ce–Fe–O system there was a variation of n values from 0.02 up to 0.3 (Table 3). The apparent reaction orders m and n are shown in Fig. 2 as a function of reaction temperature.

Rideal–Eley mechanism

Here, in a second approach, the reaction rate is expressed by the Rideal–Eley mechanism where adsorbed oxygen, in dissociative form, is assumed to react with gaseous methane:

$$R = \frac{k(K_{\text{O}_2}P_{\text{O}_2})^{1/2}P_{\text{CH}_4}}{1 + (K_{\text{O}_2}P_{\text{O}_2})^{1/2}} \quad (3)$$

where k is the rate constant, K_{O_2} is the adsorption equilibrium constant of oxygen and $P_{\text{O}_2} = P_{\text{O}_2}^\circ(P_{\text{O}_2}^\circ/P_{\text{CH}_4}^\circ - 2x)$, $P_{\text{CH}_4} = P_{\text{CH}_4}^\circ(1 - x)$ were $P_{\text{O}_2}^\circ$, $P_{\text{CH}_4}^\circ$ are the initial partial pressures of oxygen and methane, respectively, and x is the methane

Table 3 Phenomenological reaction orders m for methane and n for oxygen calculated from the straight lines of Fig. 1 (according to eqn. (2))

$\theta/^\circ\text{C}$	$\text{La}_{0.7}\text{Ce}_{0.3}\text{FeO}_3$		$\text{La}_{0.7}\text{Sr}_{0.3}\text{FeO}_3$		$\text{La}_{0.7}\text{Sr}_{0.1}\text{Ce}_{0.2}\text{FeO}_3$	
	m	n	m	n	m	n
440	0.79 ± 0.02	0.41 ± 0.02	0.72 ± 0.05	0.14 ± 0.01	0.73 ± 0.05	0.08 ± 0.00
460	0.69 ± 0.03	0.29 ± 0.03	0.67 ± 0.04	0.28 ± 0.05	0.64 ± 0.03	0.31 ± 0.03
480	0.74 ± 0.05	0.27 ± 0.02	0.77 ± 0.04	0.16 ± 0.06	0.77 ± 0.05	0.18 ± 0.05
500	0.74 ± 0.02	0.28 ± 0.02	0.68 ± 0.09	0.09 ± 0.05	0.70 ± 0.03	0.02 ± 0.09
540	0.80 ± 0.03	0.34 ± 0.04	0.80 ± 0.03	0.10 ± 0.03	0.75 ± 0.02	0.04 ± 0.09
580	0.81 ± 0.02	0.37 ± 0.02	0.81 ± 0.02	0.10 ± 0.03	0.78 ± 0.06	0.10 ± 0.09
620	0.82 ± 0.01	0.46 ± 0.06	0.82 ± 0.02	0.11 ± 0.02	0.80 ± 0.02	0.15 ± 0.08

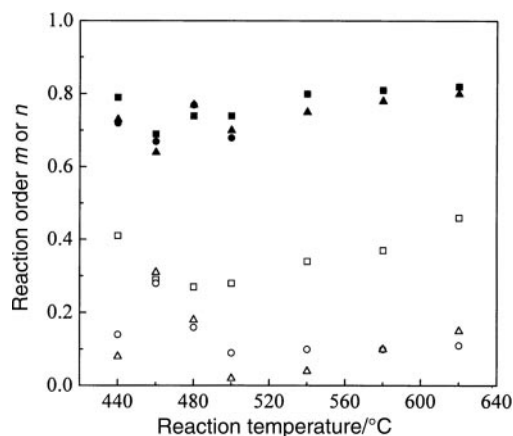


Fig. 2 Variation of apparent reaction orders n and m as a function of temperature for the three tested catalysts. Upper solid symbols: orders for methane- m ; Lower open symbols: orders for oxygen- n . Squares: $\text{La}_{0.7}\text{Ce}_{0.3}\text{FeO}_3$, circles: $\text{La}_{0.7}\text{Sr}_{0.3}\text{FeO}_3$ and triangles: $\text{La}_{0.7}\text{Sr}_{0.1}\text{Ce}_{0.2}\text{FeO}_3$.

conversion according to the reaction $\text{CH}_4 + 2\text{O}_2 \rightarrow \text{CO}_2 + 2\text{H}_2\text{O}$. Similar kinetics have been used in the past by various researchers.^{3,6,16}

The experimental results for the three examined catalysts are shown as points in Fig. 3. In the same figure, the best fitting curves, according to the Rideal–Eley mechanism, (eqn. (3)), are shown as solid lines calculated using a suitable computer program.²⁰ The corresponding k and K_{O_2} constants were adjusted by an optimization subroutine of the software and they will be discussed below.

Langmuir–Hinshelwood mechanism

In a third approach the kinetics for the system under study were simulated using a Langmuir–Hinshelwood-type equation

in which the surface reaction between adsorbed methane and adsorbed oxygen is the rate-determining step:

$$R = \frac{kK_{\text{CH}_4}P_{\text{CH}_4}(K_{\text{O}_2}P_{\text{O}_2})^{1/2}}{[1 + K_{\text{CH}_4}P_{\text{CH}_4} + (K_{\text{O}_2}P_{\text{O}_2})^{1/2}]^2} \quad (4)$$

where k , K_{O_2} , K_{CH_4} , P_{O_2} and P_{CH_4} have their customary meaning and the P_{O_2} and P_{CH_4} values are calculated as previously.

Plots of the simulated reaction rate curves, according to eqn. (4), for the three examined catalysts, again using a suitable optimizing computer program,²⁰ are shown in Fig. 4 as a function of the partial pressure of methane and of oxygen. The corresponding k , K_{O_2} and K_{CH_4} were adjusted by the computer program so as to achieve the best fit in each case.

Discussion

From Figs. 3 and 4 it is clear that the experimental results follow the Rideal–Eley kinetic model (Fig. 3). On the contrary, the Langmuir–Hinshelwood model overshoots gravely the experimental data, especially at high temperatures and high conversions. Therefore we shall restrict our attention to the results obtained from the Rideal–Eley treatment (eqn. (3), Fig. 3).

The corresponding reaction rate constant k and the adsorption equilibrium constant of oxygen K_{O_2} calculated from the fitting of the experimental data with the computer simulation of eqn. (3) show a temperature dependence according to the well-known relationships

$$k = k^0 \exp(-E_a/RT) \quad (\text{Arrhenius}) \quad (5)$$

$$K_{\text{O}_2} = K_{\text{O}_2}^0 \exp(\lambda_{\text{O}_2}/RT) \quad (\text{van't Hoff}) \quad (6)$$

The relative mechanism is based on the dissociative chemisorption of oxygen molecules at some active sites over the catalyst surface. This dissociative chemisorption is regulated

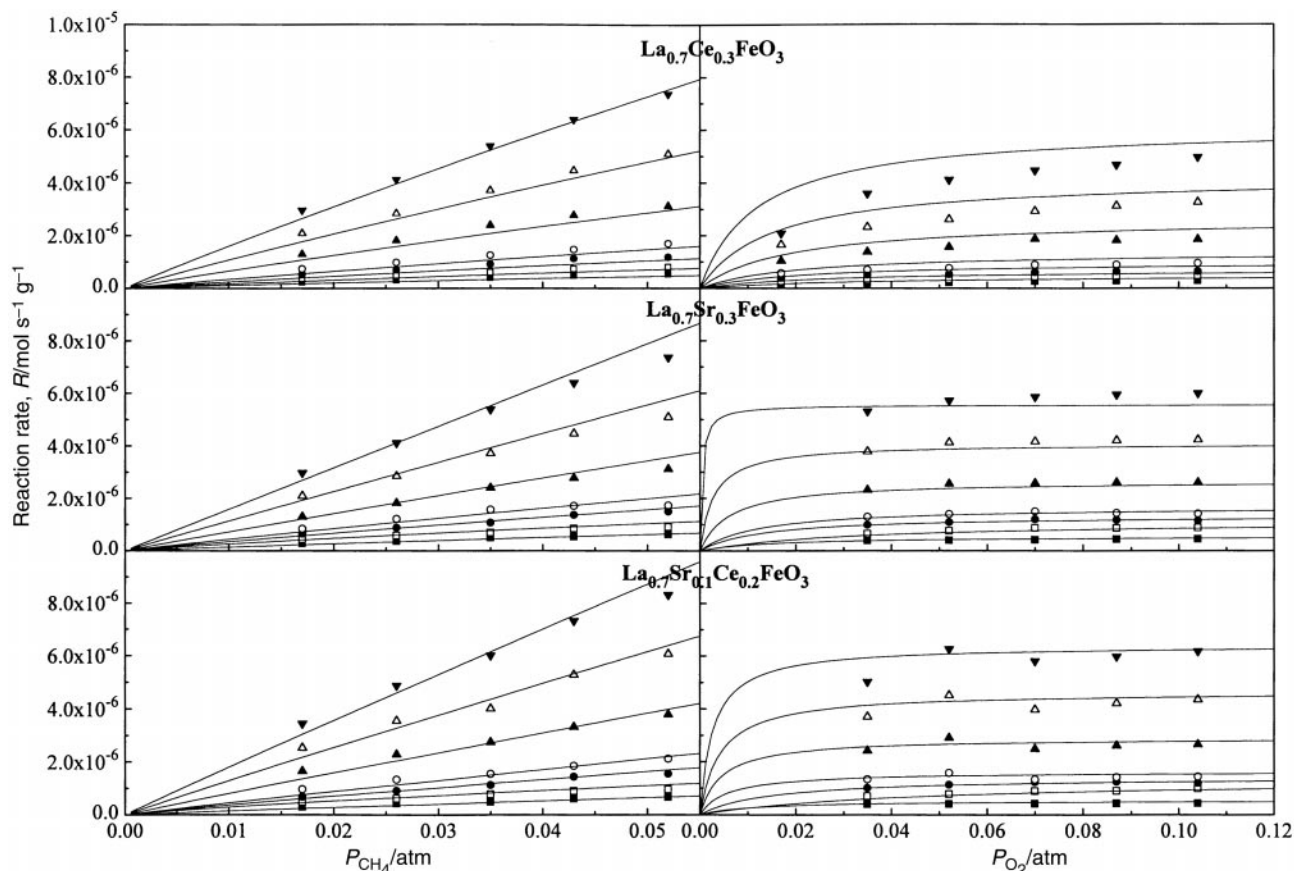


Fig. 3 Graphical representation of eqn. (3). Points: experimental; lines: best computer fittings according to the Rideal–Eley mechanism, eqn. (3), for the optimum k and K_{O_2} values. (■) 440; (□) 460; (●) 480; (○) 500; (▲) 540; (△) 580 and (▼) 620 °C.

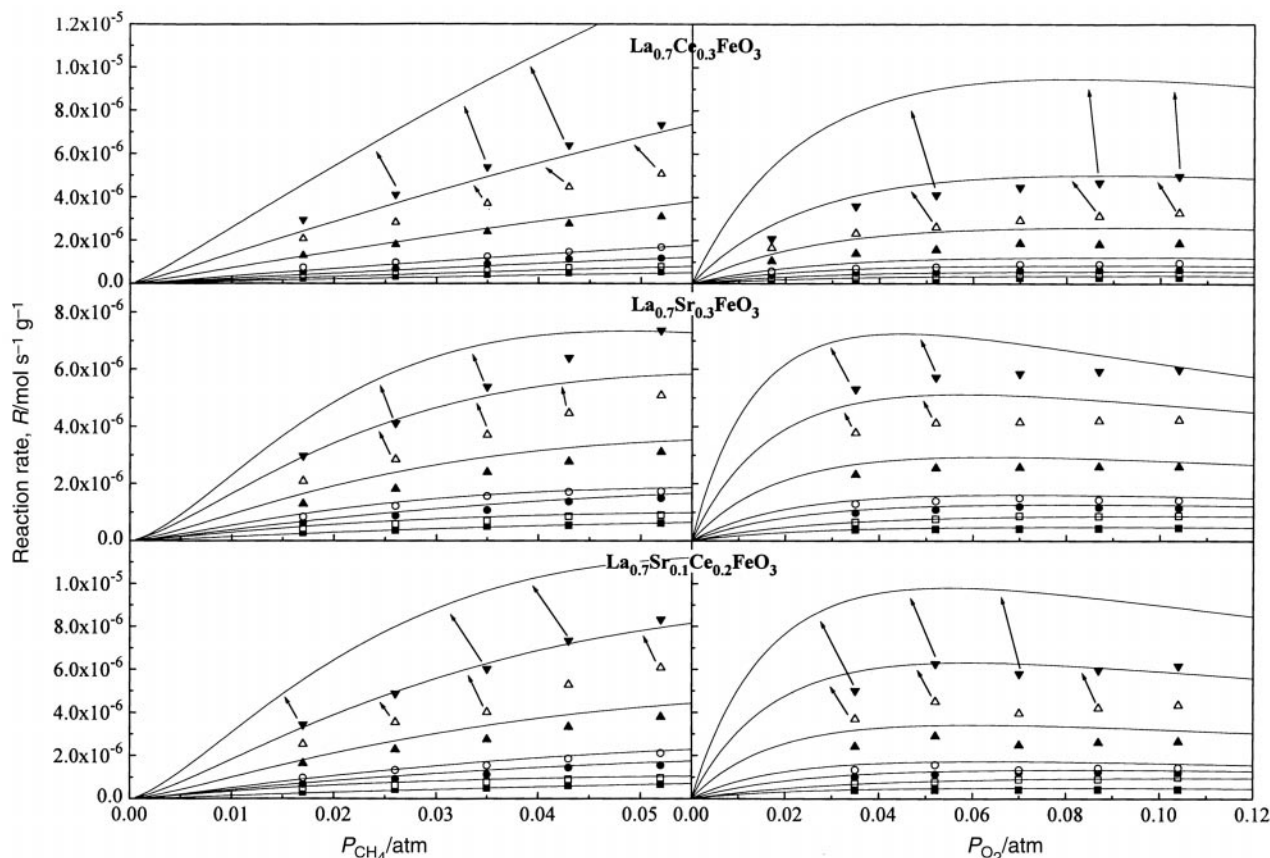


Fig. 4 Graphical representation of eqn. (4). Points: experimental; lines: best computer fittings according to the Langmuir–Hinshelwood mechanism, eqn. (4), for the optimum k , K_{O_2} and K_{CH_4} values. (■) 440; (□) 460; (●) 480; (○) 500; (▲) 540; (△) 580 and (▼) 620 °C. The arrows show the line corresponding to the experimental points.

by a van't Hoff type equilibrium expression (eqn. (6)). In this relation λ_{O_2} corresponds to the heat of dissociative adsorption of oxygen. This chemisorptive step is then followed by reaction of gaseous methane with one of the derived oxygen atoms, which initiates the combustion process with a reaction rate governed by the kinetic constant k (eqn. (5)).

The constants k and K_{O_2} in their logarithmic form, $\ln k$ and $\ln K_{O_2}$, have been plotted *vs.* $1000/T$ in Fig. 5 for the three catalysts. Good straight lines could be drawn, especially for the Arrhenius plots $\ln k = f(1000/T)$ (left-hand part in Fig. 5). For the van't Hoff plots $\ln K_{O_2} = f(1000/T)$ (right-hand part in Fig. 5) some scattering of the experimental points is apparent, especially for the Sr-containing catalysts, La–Sr–Fe–O and La–Sr–Ce–Fe–O. Such phenomena might be related to the complex dependence of k on the reaction temperature. But, in any case, the slopes can give us a fair estimation of the corresponding λ_{O_2} values. From the slopes of the correspond-

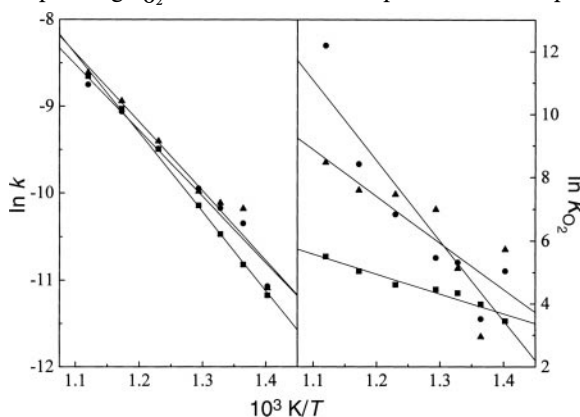


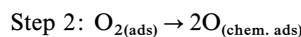
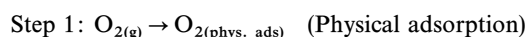
Fig. 5 Logarithmic plots of Arrhenius, eqn. (5), and van't Hoff, eqn. (6), expressions. Squares: $La_{0.7}Ce_{0.3}FeO_3$, circles: $La_{0.7}Sr_{0.3}FeO_3$ and triangles: $La_{0.7}Sr_{0.1}Ce_{0.2}FeO_3$.

ing lines the true activation energies E_{true} and the enthalpy λ_{O_2} of the dissociative adsorption of oxygen were calculated and are cited in Table 4 together with similar data from catalytic tests from other groups referring to the same reaction over perovskite-type catalysts.

It is now worthwhile comparing the experimental values of the present work with other relevant values from the literature. This can be done in Table 4 which contains true (E_{true}) and apparent (E_{app}) activation energies, as calculated by different authors using various kinetic models, as well as the heats of adsorption of oxygen λ_{O_2} found in some of these cases.

In Table 4 we observe that the data for E_{app} calculated on substituted perovskites are in most cases in the range 80–90 kJ mol^{-1} . The E_{true} values, when comparison is possible, are of the same order of magnitude, but usually smaller by 5–20 kJ mol^{-1} . Finally, the λ_{O_2} values appear to fall in two categories: one of large λ_{O_2} values around 200–300 kJ mol^{-1} and another of low λ_{O_2} values in the range 50–120 kJ mol^{-1} .

One point to be discussed here is the *positive* values found for λ_{O_2} (Table 4). Similar positive values have been observed by other authors.¹⁶ Those values mean that the dissociative adsorption of oxygen on the catalyst surface is an activated process, which can be described by the following steps



(Dissociative chemical adsorption)

Of the two steps, usually the chemical one needs activation. So the λ_{O_2} values probably correspond to such a slow and rate determining process.

One important relevant question is how these values, E_{app} , E_{true} and λ_{O_2} , are eventually interrelated, especially in the case

Table 4 Apparent and true activation energies (kJ mol^{-1}) and heats of adsorption of oxygen (kJ mol^{-1}) found using various kinetics for methane combustion

Catalyst	Kinetics employed						Ref.
	1st order	Rideal–Eley		Two term model,			
	$R = kP_{\text{CH}_4}$	$R = \frac{k(K_{\text{O}_2}P_{\text{O}_2})^{1/2}P_{\text{CH}_4}}{1 + (K_{\text{O}_2}P_{\text{O}_2})^{1/2}}$		$R_{\text{total}} = kP_{\text{CH}_4}P_{\text{O}_2}^{0.5} + k_1P_{\text{CH}_4}$			
$E_{\text{app}}/\text{kJ mol}^{-1}$	$E_{\text{true}}/\text{kJ mol}^{-1}$	$\lambda_{\text{O}_2}/\text{kJ mol}^{-1}$	$E_{\text{true}}/\text{kJ mol}^{-1}$	$\lambda_{\text{O}_2}/\text{kJ mol}^{-1}$	$E_1/\text{kJ mol}^{-1}$		
$\text{La}_{0.6}\text{Sr}_{0.4}\text{MnO}_3$	84.2			85.0	291.4	104.7	6
$\text{La}_{0.8}\text{Sr}_{0.2}\text{MnO}_3$	65.7			59.0	274.7	166.2	
$\text{La}_{1.25}\text{Sr}_{0.75}\text{NiO}_{4-n}$ ^a	—			47.4	—	110.8	13
$\text{La}_{1.25}\text{Sr}_{0.75}\text{NiO}_{4-c}$	—			61.4	—	52.5	
$\text{La}_{0.66}\text{Sr}_{0.34}\text{Ni}_{0.3}\text{Co}_{0.7}\text{O}_3$	92			92	—	92	10
$\text{La}_{0.4}\text{Sr}_{0.6}\text{Fe}_{0.4}\text{Co}_{0.6}\text{O}_3$	105			84	—	100	
LaMnO_3		149.0	98.4				16
$\text{LaMn}_{0.8}\text{Mg}_{0.2}\text{O}_3$ HT ^c		202.2	246.6				
LT ^d		121.8	18.8				
$\text{La}_{0.7}\text{Ce}_{0.3}\text{FeO}_3$	90.2	75.5 ± 1.8	52.6 ± 5.5				This work and 12
$\text{La}_{0.7}\text{Sr}_{0.3}\text{FeO}_3$	88.9	63.2 ± 4.9	211.1 ± 41.8				
$\text{La}_{0.7}\text{Sr}_{0.1}\text{Ce}_{0.2}\text{FeO}_3$	83.9	66.1 ± 6.5	122.3 ± 39.6				

^a Nitrate preparation route. ^b Citrate preparation route. ^c High reaction temperature. ^d Low reaction temperature.

of not so clear-cut cases where the Rideal–Eley kinetic, eqn. (3), can not be reduced to a first order relation $R = kP_{\text{CH}_4}$?

Furthermore, it can be easily appreciated that empirical kinetic equations like eqn. (1) used previously and their graphical treatment (Fig. 1, eqn. (2)) are a rough approximation of formal kinetic curves expressing Rideal–Eley kinetics (Fig. 2). Then what is the meaning of n and m in such cases? Clearly these values depend on how fast the reaction rate R approaches a steady value as the pressure P increases. In other words these phenomenological parameters m and n are related to the strength of oxygen adsorption. How? What is their influence on E_{app} ? The following treatment is an attempt to trace answers to such questions.

Eqn. (3) can be re-expressed in the form

$$R = k(K_{\text{O}_2}P_{\text{O}_2})^{1/2}P_{\text{CH}_4}^b/(K_{\text{O}_2}P_{\text{O}_2})^a \quad (7)$$

where

$$1 + (K_{\text{O}_2}P_{\text{O}_2})^{1/2} = (K_{\text{O}_2}P_{\text{O}_2})^a \quad (8)$$

In the above relationship a is real number whose value is defined by the equation $a = \ln(1 + K_{\text{O}_2}^{1/2}P_{\text{O}_2}^{1/2})/\ln(K_{\text{O}_2}P_{\text{O}_2})$ and for variations of P of less than one order of magnitude, as in the present case, can be considered to be approximately constant.

Then eqn. (7) can be written in the form

$$R = k(K_{\text{O}_2}P_{\text{O}_2})^{0.5-a}P_{\text{CH}_4}^b \quad (9)$$

and after taking logarithms

$$\ln R = \ln k + (0.5 - a)\ln K_{\text{O}_2} + (0.5 - a)\ln P_{\text{O}_2} + b \ln P_{\text{CH}_4} \quad (10)$$

Eqn. (10) is similar to eqn. (2) with

$$m = b \quad (11)$$

$$n = 0.5 - a \quad (12)$$

$$k' = kK_{\text{O}_2}^{0.5-a} = kK_{\text{O}_2}^n \quad (13)$$

Therefore from the plots given in Fig. 1 the b and a values can be found in each case. As expected $m \approx b \approx 1$ and indeed m is found in the range 0.7–0.8 (Table 3). The discrepancies from the ideal value $m = b = 1$ are due to experimental and/or systematic errors in the treatment of the data.

Of more interest is the second case where, from the slopes $n = 0.5 - a$ (Fig. 1 and Table 3), we can estimate the relationship between E_{true} and λ_{O_2} using the logarithmic form of eqn. (13)

$$\ln k' = \ln k + n \ln K_{\text{O}_2} \quad (14)$$

from which we can easily see that

$$E_{\text{app}} = E_{\text{true}} + n\lambda_{\text{O}_2} \quad (15)$$

Similar relationships have been proposed some time ago by the Novosibirsk group²³ for quite different systems using a totally different approach.

To test this hypothesis we have plotted the $\ln k'$ values corresponding to the intercepts $\ln R$ at $P_{\text{O}_2} = 0$ of the straight lines in Fig. 1, vs. $1000/T$ in Fig. 6.

We can see that fairly good Arrhenius-type straight lines are obtained and visual comparison with the relevant slopes in Fig. 5 is interesting, showing both similarities and differences. The calculated slopes from Fig. 6 should correspond to E_{app} and should be compared to the corresponding E_{app} values found via eqn. (15) using the E_{true} and λ_{O_2} values determined previously via a totally different way, i.e. the simulation in Fig. 3.

The extent to which the above can be verified is shown in Table 5 in which a comparison between the relevant results is

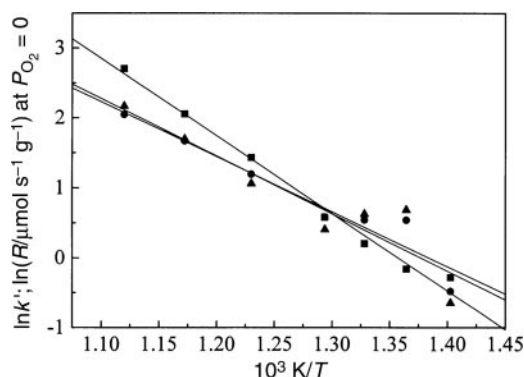


Fig. 6 Plots of the intercepts $\ln k'$ or $\ln R$ at $P_{\text{O}_2} = 0$, from Fig. 1, vs. $1000/T$. For details see text. (■) $\text{La}_{0.7}\text{Ce}_{0.3}\text{FeO}_3$, (●) $\text{La}_{0.7}\text{Sr}_{0.3}\text{FeO}_3$ and (▲) $\text{La}_{0.7}\text{Sr}_{0.1}\text{Ce}_{0.2}\text{FeO}_3$.

Table 5 Comparison of data for the interrelation of E_{app} , E_{true} , n and λ_{O_2}

Method of estimation	$E_{\text{app}}/\text{kJ mol}^{-1}$		
	$\text{La}_{0.7}\text{Ce}_{0.3}\text{FeO}_3$	$\text{La}_{0.7}\text{Sr}_{0.3}\text{FeO}_3$	$\text{La}_{0.7}\text{Sr}_{0.1}\text{Ce}_{0.2}\text{FeO}_3$
Slopes of $\ln R = f(1000/T)$ from ref. 12	90.2	88.9	83.9
Eqn. (15) using n values found from Fig. 1, eqn. (2) and the λ_{O_2} and E_{true} values found from Fig. 5, eqn. (5)	93.6 ^a	92.7 ^b	82.0 ^c
Plots in Fig. 6	92.3	65.3	68.4

^a $E_{\text{app}} (\text{kJ mol}^{-1}) = E_{\text{true}} + n\lambda_{\text{O}_2}$; $93.9 = 75.5 + (0.35 \times 52.6)$. ^b $94.15 = 63.2 + (0.14 \times 221.1)$. ^c $82.0 = 66.1 + (0.13 \times 122.3)$.

shown. This table contains the E_{app} values found by three different ways for the three tested catalysts: First E_{app} as found from the slopes of the Arrhenius-type lines in ref. 12. Second the E_{app} values as found from eqn. (15) after substituting the relevant values of E_{true} , the mean value of the reaction rate order n and λ_{O_2} calculated previously in this work. Third the E_{app} values calculated from the Arrhenius-type plots in Fig. 6.

The agreement between these values is excellent for the La–Ce–Fe–O catalysts for the three cases. In the other two cases (catalysts La–Sr–Fe–O and La–Sr–Ce–Fe–O) the plots in Fig. 6 give lower values as compared to the other two methods of calculation. These discrepancies can be traced to the less satisfactory matching of the lines in Fig. 1 with the actual Rideal–Eley curves in Fig. 3.

In other words when the reaction rate R , as described by the Rideal–Eley scheme, increases in a smooth way as a function of P_{O_2} , as observed in the case of La–Ce–Fe–O (Fig. 3), then the matching between the three cases is perfect. On the other hand if the values of R , as a function of P_{O_2} , quickly reach steady values, as in the case of La–Sr–Fe–O and La–Sr–Ce–Fe–O solids, an appreciable mismatching is developed between the calculated values of E_{app} , because the exponential eqn. (9) expresses the situation in a less satisfactory way. In those cases the values of E_{app} from the other two methods should be nearer to the actual value.

Therefore eqn. (9) is more applicable and useful in cases where KP values in the denominator of the Rideal–Eley relationship are of the same order of magnitude as unity. In other words, when KP is relatively small but not too small. When KP is getting larger and larger, eventually the model ceases to express the kinetics.

What might be the physicochemical reasons for the stronger adsorption of oxygen on the La–Sr–Fe–O and La–Sr–Ce–Fe–O solids, which lead to larger values of the $K_{\text{O}_2}P_{\text{O}_2}$ term in the Rideal–Eley relationship and to the fast approach of steady values of reaction rate R as a function of P_{O_2} in Fig. 3? We think that this is related to the existence of a $\text{SrFeO}_{3\pm x}$ crystal phase in the two solids. This crystal phase was determined previously^{17,18} very precisely with Mössbauer spectroscopy at 20 K and the results are listed in Table 1. We observe in this table that La–Sr–Fe–O contains 33% of $\text{SrFeO}_{3\pm x}$ while La–Sr–Ce–Fe–O contains 12% of this phase. Furthermore the phase $\text{SrFeO}_{3\pm x}$ was found to be directly related to the extensive oxygen uptake as determined by O_2 -TPD experiments.¹⁸ This strong and extensive adsorption of oxygen on the $\text{SrFeO}_{3\pm x}$ crystal phase of those two solids La–Sr–Fe–O and La–Sr–Ce–Fe–O, justifies the large $K_{\text{O}_2}P_{\text{O}_2}$ values and their different behaviour compared to the La–Ce–Fe–O sample.

Conclusions

The following conclusions can be drawn from this work.

The kinetics of the deep oxidation of CH_4 on oxidic solids La–Ce–Fe–O, La–Sr–Fe–O and La–Sr–Ce–Fe–O, having mixed oxidic and perovskitic components, follow the Rideal–Eley model.

A simulation of the kinetic results using a suitable computer program²⁰ enables the direct estimation of kinetic and equilibrium constants as well as the determination of true activation energies E_{true} and the heats of adsorption of oxygen λ_{O_2} .

The exponent n used in the empirical rate equation $R = k'(P_{\text{O}_2})^n(P_{\text{CH}_4})^m$ can be related to the extent of contribution of the heat of adsorption λ_{O_2} to the apparent activation energy according to the relationship $E_{\text{app}} = E_{\text{true}} + n\lambda_{\text{O}_2}$. This is applied more precisely in cases where the $K_{\text{O}_2}P_{\text{O}_2}$ term is of the same order of magnitude as unity, while some discrepancies develop as soon as $K_{\text{O}_2}P_{\text{O}_2}$ becomes larger and larger.

Large values of K_{O_2} and λ_{O_2} for the above solids were related to the existence of a $\text{SrFeO}_{3\pm x}$ perovskite crystal phase, which is able to uptake large amounts of oxygen as established by TPD/ O_2 experiments in previous work.¹⁸

References

- M. F. M. Zwinkels, S. G. Jaras and P. G. Menon, *Catal. Rev.-Sci. Eng.*, 1993, **35**, 319.
- Advanced Materials in Catalysis*, ed. R. J. H. Voorhoeve, J. P. Remeika and L. E. Trimble, New York, 1977, p. 129.
- L. G. Tejuka, J. L. G. Fierro and J. M. D. Tascon, *Adv. Catal.*, 1989, **36**, 237.
- J. G. McCarty and H. Wise, *Catal. Today*, 1990, **8**, 231.
- T. Seiyama, *Catal. Rev.-Sci. Eng.*, 1992, **34**, 281.
- H. Arai, T. Yamada, K. Eguchi and T. Seiyama, *Appl. Catal.*, 1986, **26**, 265.
- M. Stojanovic, C. M. Mims, H. Moudallal, Y. L. Yang and A. J. Jacobson, *J. Catal.*, 1997, **166**, 324.
- L. Marchetti and L. Forni, *Appl. Catal. B*, 1998, **15**, 179.
- H. M. Zhang, Y. Shimizu, Y. Teraoka, N. Miura and N. Yamazoe, *J. Catal.*, 1990, **121**, 432.
- D. Klvana, J. Vaillancourt, J. Kirchnerova and J. Chauki, *Appl. Catal. A*, 1994, **109**, 181.
- Y. Teraoka, H. M. Zhang and N. Yamazoe, *Chem. Lett.*, 1985, 1367.
- V. C. Belessi, A. K. Ladavos and P. J. Pomonis, *Appl. Catal. B: Environmental*, 2001, **31**, 183.
- A. K. Ladavos and P. J. Pomonis, *J. Chem. Soc., Faraday Trans.*, 1992, **88**, 2557.
- Y. Yao, *Ind. Eng. Chem., Prod. Res. Dev.*, 1980, **19**, 293.
- K. Otto, J. M. Andino and C. L. Parks, *J. Catal.*, 1991, **131**, 243.
- G. Saracco, F. Geobaldo and G. Baldi, *Appl. Catal. B*, 1999, **20**, 277.
- V. C. Belessi, C. N. Costa, T. V. Bakas, T. Anastasiadou, P. J. Pomonis and A. M. Efstathiou, *Catal. Today*, 2000, **59**, 347.
- V. C. Belessi, T. V. Bakas, C. N. Costa, A. M. Efstathiou and P. J. Pomonis, *Appl. Catal. B*, 2000, **28**, 13.
- G. Longworth, in *Mössbauer Spectroscopy Applied to Inorganic Chemistry*, ed. E. J. Long, Plenum Press, New York, 1984, vol. I, p. 43.
- The relevant computer program is available on request from ppomonis@cc.uoi.gr
- Y. Bard, in *Non Linear Parameter Estimation*, Academic Press, New York, 1973, p. 83.
- D. Cuthbert, F. Wood and J. Gorman, in *Fitting Equations to Data: Computer Analysis of Multifactor Data*, John Wiley & Sons, New York, 2nd edn., 1999.
- G. K. Boreskov, V. V. Popovski and V. A. Sazonov, *Proceedings of the 4th International Congress Catalysis*, Moscow, 1968, p. 439.